International Journal of Geo-Engineering

TECHNICAL REPORT Open Access

Usage of permeability ratio to check the stability of a pile-soil model with retaining wall support – Huizhou slope failure as a case study

Muhammad Israr Khan[1], Jianbo Fei[1*], Xiangsheng Chen[1] and Yue Chen[2]

*Correspondence:
Jianbo Fei
feijianbo@szu.edu.cn
[1]Key Laboratory of Coastal Urban Resilient Infrastructures, College of Civil and Transportation Engineering, Shenzhen University, Shenzhen 518060, China
[2]Central Research Institution of Building and Construction Co., Ltd, MCC Group, Shenzhen 518055, China

Abstract

This paper presents a comprehensive investigation into the role of soil permeability variation on the stability of slopes reinforced by retaining walls, with a focus on the Huizhou slope failure as a case study. The study demonstrates that rising groundwater levels diminish the Factor of Safety (FoS) for retaining walls, with stability most compromised under combined loading from adjacent soil and lightweight concrete. These findings emphasize the need for enhanced drainage or structural support in retaining wall designs subjected to elevated groundwater conditions. It integrates advanced numerical simulations, utilizing Abaqus and GeoStudio, with empirical field data to analyze the interactions between soil permeability, pore water pressure, moisture content, shear strength, and the overall stability of the slope. The dynamics of water infiltration are influenced by permeability, moisture content, and the groundwater table. These factors change the pore pressure and decrease shear strength, which causes shear failure in the slope mass. This research also looks at how surcharge loading affects slope stability. Higher permeability soils cause faster infiltration rates, leading to higher pore pressures, lower effective shear strengths, and a higher likelihood of slope failure. The opposite is true for reduced permeability, which makes drainage more difficult and ultimately leads to hydrostatic pressure building up behind retaining walls, which in turn makes the slope even more unstable. This study demonstrates the critical need for optimized drainage systems to reduce the hazards of infiltration-induced failure and the role of precise permeability evaluation in geotechnical design. Geotechnical engineers can use these results to better understand how to construct and maintain slope stabilization systems.

Keywords Slope stability, Soil permeability, Retaining walls, Groundwater dynamics, Pore water pressure

Introduction

In the field of geotechnical engineering, slope stability is a basic problem, particularly in places that are prone to experiencing seismic activity or excessive rainfall. There are a number of elements that can have a substantial impact on the stability of slopes. These

Springer Open

© The Author(s) 2025. **Open Access** This article is licensed under a Creative Commons Attribution 4.0 International License, which permits use, sharing, adaptation, distribution and reproduction in any medium or format, as long as you give appropriate credit to the original author(s) and the source, provide a link to the Creative Commons licence, and indicate if changes were made. The images or other third party material in this article are included in the article's Creative Commons licence, unless indicated otherwise in a credit line to the material. If material is not included in the article's Creative Commons licence and your intended use is not permitted by statutory regulation or exceeds the permitted use, you will need to obtain permission directly from the copyright holder. To view a copy of this licence, visit http://creativecommons.org/licenses/by/4.0/.

factors include the soil properties, the geometry of the slope, and the presence of water. Among these, the permeability of the soil is one of the most important factors in influencing the rate at which water penetrates and drains through the soil. This factor has a direct impact on the pore water pressure and shear strength of the soil. In order to build efficient retaining structures and prevent slope failures, which can have severe effects for infrastructure and safety, it is vital to have a solid understanding of how changes in permeability impact slope stability.

To describe the impact of permeability on slope stability, the Huizhou slope failure is an important case study to include in the analysis. In 2023, a catastrophic slope failure struck the city of Huizhou, located in the province of Guangdong in China, causing immense property damage and posing serious hazards to human life.

One of the most prominent applications of retaining walls is to provide support for slopes and to avoid landslides. However, the design of these walls heavily relies on the soil conditions they aim to preserve. For instance, the permeability-governed interaction between water and soil can lead to fluctuations in the water pressure within the pores, thereby impacting the structural integrity of these structures. The quick penetration of water into soils with high permeability can lead to an increase in pore water pressures and a decrease in soil shear strength, both of which can result in instability. On the other hand, soils with low permeability have the potential to hold water for longer periods of time, which consequently results in prolonged high pressures behind the retaining wall. Therefore, in order to design and install successful retaining structures, it is essential to have a comprehensive understanding of the role that permeability has in slope stability.

New techniques for building reinforced earth retaining walls have been researched and tested in the field due to the fact that there have been numerous examples where a partial collapse of a reinforced front wall causes the entire reinforced earth structure with a steep soil slope to collapse. Suppressing the bulging phenomena of front walls that happens during construction is the subject of several research that aim to determine its economic feasibility and safety [1–5].

As studies proved that one of the main reasons behind the slope failure is the permeability variation due to rainfall events [6–8]. Regions with clay-rich soils are particularly susceptible to hazards caused by landslides triggered by rainfall. This is because water infiltration can have a profound impact on the permeability and stability of the ground. Clay, characterized by its small particles and great ability to be molded, reacts distinctively to rainfall, affecting its ability to allow water to pass through and causing landslides in specific circumstances. As a result of increased research conducted over the past few decades, it has been established beyond any doubt that the primary failure mechanisms of rainfall-triggered landslides are the loss of matric suction in unsaturated soil, the development of porewater pressure, and the reduction of saturation-dependent shear strength. This is in addition to the fact that adverse geological and topographic features are a contributor to the initiation of landslides. Through the utilization of a variety of techniques, such as numerical modelling and simulations [8, 9], model testing [10, 11], field testing [12–14] and small or large scale testing [15, 16], a significant advancements have been made in the investigation of landslides or slope failures that are caused by rainfall. Clay-based soils have low permeability because of their compact structure, which makes it difficult for water to travel through them. However, prolonged or strong rainfall can cause these soils to become saturated, leading to an increase in

pore water pressure and a decrease in their shear strength. This rise in pore pressure reduces the effective stress within the soil mass, a crucial factor in determining the soil's stability. Water that penetrates clay-rich slopes during periods of high rainfall has the potential to damage the structure of the soil, which might result in landslides. Significant changes in clay permeability due to rainfall can make the slope unstable. A landslip often disrupts the natural layering and compaction of clay soils, altering the permeability properties of the surrounding soil. This disturbance may create preferential pathways for water infiltration, potentially leading to an increase in the permeability of the affected clay layers. To analyze landslide hazards and reduce their repercussions, it is essential to have a solid understanding of these processes. Various geologists and engineers analyze the changes in clay permeability after a landslide to predict future instability and develop suitable strategies for slope stabilization [17, 18]. Intense rainfall events caused fewer landslides than uniform rainfall events because of decreased rainfall infiltration, according to research by a researcher [19] on the temporal pattern of rainfall and landslide occurrences. The total amount of rainwater remained the same in both cases. Retrogressive failure at the same rainfall intensity (90 mm/h) has been observed by Miao et al. [20] on the slope with a high fine particle content. Wang et al. [21] studied the effect of the rainfall intensity/permeability coefficient ratio (q/k) on the infiltration properties of the slope. The researchers found that infiltration capacity improves with rainfall intensity when q/k < 1 and decreases when q/k > 1. With a rainfall intensity of 25 mm/h, Hsu et al. [22] conducted model studies on slopes with silty sand. According to Locat et al. [23] and Shan et al. [24], the instability happened in a retrogressive failure mode where the slippage started at the base of the slope and worked its way up to the crest. Despite using silty clay soil and a substantially higher rainfall intensity of 72 mm/h, Wu et al. [25] found a comparable failure mode in their model slope testing. Over the past few decades, researchers have conducted both theoretical and experimental research to investigate the mechanisms causing shallow landslides caused by rainfall [26–37]. Slope stability analysis with from different aspects is also studied, investigated and concluded with very useful results is published in different journals [38–47]. Another research also explores the response of soft clay soils beneath Qasr Yashbak using numerical modeling, offering insights into their behavior and the reduction in soil-bearing capacity caused by variations in moisture levels or fluctuations in the groundwater Table [48]. Similarly, another researcher used Artificial Intelligence techniques to study the stabilization of soil and predict the embedment depth for cantilever sheet pile walls in cohesive soils, with a particular focus on the influence of cohesionless soil backfill [49].

There has been a lack of concurrent model test investigations that could shed light on the respective roles played by rainfall intensity and soil permeability in determining the manner of slope failure. This paper aims to explore the impact of permeability variation on the stability of slopes supported by retaining walls, with a focus on the Huizhou slope failure as a case study. Through numerical modeling and field data analysis, the study examines how different permeability conditions affect pore water pressure, shear strength, and overall slope stability. By identifying the mechanisms through which permeability influences these factors, the research seeks to provide geotechnical engineers with insights that can improve slope design and enhance the resilience of retaining structures. Ultimately, the findings of this study aim to contribute to safer and more effective slope management practices in geotechnically challenging environments. The

Fig. 1 Site location [50]

Fig. 2 Retaining wall failure direction

project location for Daya Bay Binhe Road Phase II (Zhongxing 2nd Road to Baishouwan Bridge Section) can be found in the central north region of Aotou Street, which is located in the Daya Bay District of Huizhou city. It can be found along the road on both sides of the Tamao River, which is located to the west. Binhe South Road (Xin'ao Avenue to Yiyuan Road Section), Binhe South Road (Zhongxing 5th Road to Baishouwan Bridge Section), and Binhe North Road (Zhongxing 5th Road to Baishouwan Bridge Section) are the three sub-projects that are included in the design scope of this project. These sub-projects are included in accordance with the requirements of the design, planning, and design conditions of Daya Bay Binhe Road Phase II. Figure 1 shows the Huizhou slope location and Fig. 2 shows the picture of the failed retaining wall due to the slope instability.

Fig. 3 (**a** and **b**) Cracks appeared to the left side of the slope and the slope's middle part after failure respectively

Fig. 4 (**a**, **b**) Top view and side view of the slope and retaining wall respectively

The slope in question was supported by a concrete retaining wall, yet the failure occurred, suggesting that underlying geotechnical factors were not adequately addressed. Figure 3 (a and b) shows the cracks appeared to the left side of the slope and the slope's middle part after failure respectively.

Figure 4 (a and b) shows the top view and side view of the slope after failure respectively.

This incident underscores the need for a detailed investigation into how variations in soil permeability might have contributed to the failure, providing valuable lessons for future slope stabilization projects.

A visit was scheduled to the site on October 13, 2023, to examine it and collect samples for evaluation. The slope collapsed due to a profound slippage, most likely marked by a circular slip surface. Uncertainty about the reasons for the failure and slippage prompted a review of all pertinent literature in the field of retaining walls and piles. Next, we examined the slope using 3D slope stability analysis software, considering the relevant literature. The primary objectives of this study are (1) to identify the factors that cause the slope to slide and fail, and (2) to provide an optimal strategy for stabilizing the slope and retaining wall to prevent future failures of such models and slips.

Material properties and Testing

Static penetration testing is an in-situ testing method for foundation soil. Its testing principle is to use pressure equipment (static penetration instrument) to press the probe into the soil, and use measuring instruments to record and display the soil penetration resistance (including cone tip resistance and side wall friction resistance). Through analysis and calculation, geological stratification and strength parameters are obtained. According to relevant specifications and technical requirements, the instruments were checked and the probes were calibrated before the test. During the test, the penetration speed of the static penetration test was controlled within the range of (1.2 ± 0.3) m/min. It meets the requirements of relevant specifications for penetration speed. This test was conducted in accordance with the relevant provisions of the national standard "Geotechnical Engineering Investigation Code" (GB 50021 – 2001) [51]. Samples taken from eight number of boreholes at different points. The slip area measures approximately 164 ft (50 m) in length and 36 ft (11 m) in width. Static penetration tests (SPTs) are typically conducted at intervals ranging from 30 to 50 ft in areas with uniform soil conditions. Accordingly, three SPT locations were selected across the slope's length, spaced approximately 50 ft apart. The testing points were strategically positioned at the beginning, midpoint, and endpoint of the slope, covering the entire range from 1 to 164 ft. Figure 5 (a and b) shows the samples taken at borehole 1. Other samples are mentioned in Annex 1.

Some basic equations used for calculating the different parameters required for the model analysis are:

$$\phi_m = \frac{\sum_{i=1}^{n} \phi_i}{n} \tag{1}$$

$$\sigma_f = \sqrt{\frac{1}{n-1}\left[\sum_{i=1}^{n} \phi_i^2 - \frac{\left(\sum_{i=1}^{n} \phi_i\right)^2}{n}\right]} \tag{2}$$

$$\delta = \frac{\sigma_f}{\phi_m} \tag{3}$$

$$\phi_k = \gamma_s \phi_m \tag{4}$$

Fig. 5 (a and b) Photos of the core from borehole 1 respectively. **a** Clayey sand samples collected at a depth of 5, 10, 15 and 20 m. **b** Motorized drilling rig equipment at borehole 1 for collecting the samples

Table 1 Relationship between the characteristic value f_{ak} of foundation (soil) bearing capacity and the standard value of specific penetration resistance (p_s) or cone tip resistance (unit: kPa)

f_{ak}	p_s	Soil type
$0.112p_s+5$	85～800	Soft soil (silt, muddy soil)
$0.02p_s+59.5$	1000～15000	Fine sand
$0.036p_s+76.6$	1000～10000	Coarse sand
$0.036p_s+44.6$	/	Silt
$5.8p_s^{0.5}$-46	≤6000	General clay soil
$0.094p_s+18.8$	2000～6000	Old clay soil

Table 2 Relationship between deformation modulus E_0 and standard value of specific penetration resistance (p_s) or cone tip resistance (unit: MPa)

E_0	p_s	Soil type
$6.03p_s^{1.45}$+0.8	0.085～2.5	Soft soil, saturated clay soil
$11.78p_s$-4.69	3～6	Clay soil
$3.57p_s^{0.684}$	1～20	Fine sand, silt sand, silt soil

$$\gamma_s = 1 - \left\{ \frac{1.704}{\sqrt{n}} + \frac{4.678}{n^2} \right\} \delta \tag{5}$$

Where: ϕ_i—— Test value or test correction value of test data;

ϕ_m—— The average value of the test data;

σ_f—— Standard deviation of test data;

δ —— Coefficient of variation of test data;

n—— Number of detection holes;

ϕ_k——Standard value of test data;

γ_s—— Statistical correction factor.

According to the national standard "Geotechnical Engineering Investigation Code" (GB 50021 – 2001), and referring to the Guangdong Provincial Standard [52] "Building Foundation Testing Code" (DBJ/T 15-60-2019), the foundation (soil) bearing capacity characteristic value f_{ak} and deformation modulus E_0 can be estimated according to Tables 1 and 2 based on the standard value of specific penetration resistance or cone tip resistance (when using the q_c value, take p_s=1.1q_c).

Through on-site in-situ testing of foundation soil, the test results were organized into static penetration test record tables, depth H ~ cone tip resistance q_c, depth H ~ side wall friction resistance f_s, depth H ~ friction resistance ratio α curves, and soil layers were divided according to the relationship curve between specific penetration resistance and depth combined with geotechnical engineering exploration data. First, the cone tip resistance and side friction resistance of each test hole were statistically analyzed according to the divided soil layers (Table 3). When counting, the values within the critical depth and the abnormal values within the leading and lagging influence range were eliminated. Then, according to the average values of the cone tip resistance and side friction resistance of the same soil layer of each test hole (excluding abnormal values), the standard values of the static penetration cone tip resistance and side friction resistance of the same soil layer of the unit project were obtained (Table 4).

Other testing details and parameters obtained from field and laboratory testing are available in Annex 2. The required material properties used in the analysis are given in Table 5.

Table 3 Statistics of the number of penetration hammer blows for each test hole

S. No.	Borehole Number	Parameter	Number count	Statistical scope	Average value
1	BH1 (Silt soil) 7.5m～16.8m	Cone tip resistance q_c (MPa)	94	0.24～0.40	0.32
		Lateral friction f_s (kPa)	94	20.7～39.7	30.4
2	BH3 (Silt soil) 7.8m～17.6 m	Cone tip resistance q_c (MPa)	99	0.19～0.35	0.27
		Lateral friction f_s (kPa)	99	19.4～39.2	30.07

Table 4 Statistics of static penetration hammer blows for unit projects

S. No.	Location	Number of holes	Parameter	Statistical scope	average value	Standard Deviation	Coefficient of variation	Correction factor	Standard value
1	Silt soil layer	2	Cone tip resistance q_c (MPa)	0.19～0.40	0.29	0.06	0.21	0.97	0.28
			Lateral friction f_s (kPa)	19.4～39.7	30.21	5.09	0.17	0.98	29.61

Table 5 Material properties used in the analysis

S. No.	Description	Mass Density (kN/m^3)	Elastic Properties		Mohr-Coulomb Plasticity			
			Young's Modulus (N/m^2)	Poisson's Ratio	Cohesion		Plasticity	
					Cohesion yield stress (kPa)	Absolute Plastic Strain	Friction (degree)	Dilation Angle (degree)
1	L1	1.9	2400	0.25	12	0	32	0.1
2	L2	1.8	2500	0.32	10	0	18	0.1
3	L3	2	28,000	0.2	12	0	40	0.1
4	L4	2.1	35,000	0.2	14	0	41	0.1
5	L5	2.2	40,000	0.2	18	0	46	0
6	F	1.5	35,000	0.3	0	0	48	0
7	LSS	2	25,000	0.2	0.4	0	1.2	0
8	RSS	2	25,000	0.2	6	0	37	0.1

The mass density for concrete made components is 2500 kg/m^3 and its Young's Modulus is 20 GPa. While for light weight concrete, the mass density is 1350 kg/m^3 and its Young's Modulus is 10 GPa. The boundary conditions include fixed at bottom in both x and y direction. And allow movement in x direction at the sides.

Results and discussion

Abaqus 2023, a finite element program used to figure out stresses, strains, displacements, safety factors, and other needed parameters, is used to model the whole model while taking all the geological conditions into account. The input parameters required by the finite element software (3D version) are Poisson ratio (ν), Young's Modulus (E), density of concrete and soil, angle of internal friction (ϕ) and cohesion (c) of soil. The overall model has different parts, i.e., Left Side Soil (LSS), Piles under Utility Tunnel (UT), Piles under Light Weight Concrete (LWC), Piles under Retaining Wall (RW), five layers of soil (L1-L5), Utility Tunnel Cover (UTC), Light Weight Concrete (LWC), Right Side

Soil (RSS), Filter (F) and Retaining Wall (RW). Figure 6 shows the 3D model of the slope build on Abaqus.

The powerful software suite known as Abaqus was developed by Dassault Systèmes Simulia Corporation for the purpose of performing Finite Element Analysis (FEA). For the purpose of studying complicated phenomena such as soil slopes and landslides, it is extensively utilized across a wide range of engineering disciplines, including civil and geotechnical engineering. With the help of Abaqus, engineers are able to do finite element analysis in three dimensions, which allows them to simulate landslide-prone locations and soil slopes. For the purpose of modelling the response to various stresses, the complex geometry is initially discretely broken down into smaller components. The Abaqus 3D software is an indispensable tool for carrying out finite element assessments of soil slopes and landslides that are particularly precise and accurate. It provides engineers and geotechnical experts with assistance in comprehending the complex relationships that exist between the behavior of soil, the external factors, and the responses of structures, thus assisting in the development of engineering designs and mitigation techniques that are safer and more effective. Abaqus is utilized in order to generate a three-dimensional model of the slope and to evaluate the stability of the slope in relation to changes in permeability. Changes in clay permeability due to rainfall can have a significant impact on the soil's behavior as well as the stability of slopes. These changes can also significantly increase the likelihood of landslides occurring. Clay soils, characterized by their small particles and strong ability to change shape, display intricate hydraulic properties when exposed to different levels of moisture. When it rains, the water seeps into the ground, causing the pressure of the water in the soil to grow. This can weaken the soil's ability to resist forces and make it more likely to become unstable. The rate at which water may move through clay soil is determined by its permeability, which is commonly represented by the mathematical symbol k. This permeability is subject to fluctuate as a result of variations in effective stress, saturation levels, and the structure of the clay matrix among other factors. There are empirical and theoretical models that can be used to characterize the relationship between permeability (k) and volumetric water content (θ) in clay.6

$$Ra = \frac{1}{N} \sum_{i=1}^{N} |\mathrm{Yi}| \tag{6}$$

where:

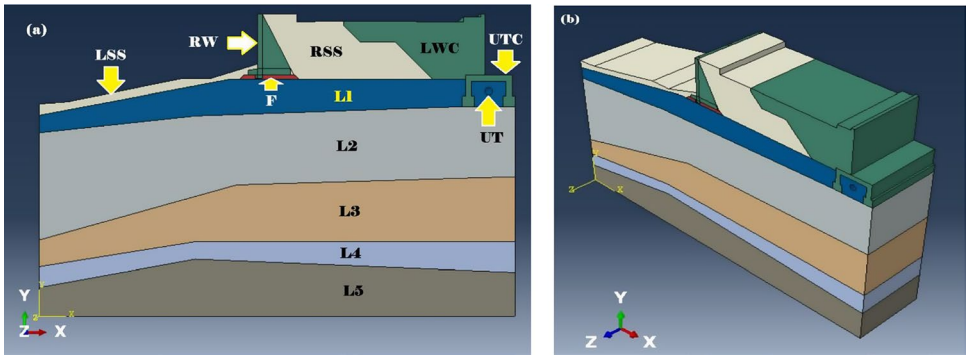

Fig. 6 Slope model (3D)

- k_0 is the initial permeability coefficient,
- θ is the volumetric water content,
- n is an empirical coefficient that depends on the soil type and structure.

Soil swelling and pore blockage cause clay to initially have a lower permeability when it absorbs water during rainfall. Permeability may rise, though, when water-filled channels form in the soil matrix in response to persistent wetness and saturation. Soil stability in slope and landslide assessments is affected by transient hydraulic conditions, and this behavior of dynamic permeability is essential for assessing these situations. The Kozeny-Carman equation relates permeability (k) to porosity (n) and specific surface area (S) of the soil particles:7

$$k = C \cdot S^2/(1-n)^2 \cdot n^3 \tag{7}$$

where:

- C is a dimensionless constant.

This equation indicates that as porosity increases due to water absorption during rainfall, the permeability of the soil typically increases, assuming the specific surface area remains constant. Considering the effect of void ratio (e) on permeability, the modified Kozeny-Carman equation is given by:8

$$k = C\prime \cdot (e \cdot S)^2/(1-n)^2 \cdot n^3 \tag{8}$$

where:

- C' is another dimensionless constant.

This modification accounts for changes in void ratio as clay swells or compacts with varying moisture content, affecting the soil's hydraulic conductivity. The Bouwer and Rice equation relates the permeability (k) to the volumetric water content (θ) and effective porosity (n):9

$$k = k_s \cdot [(\theta - \theta r)\,/\,(\theta s - \theta r)]^b \tag{9}$$

where:

- k_s is the saturated hydraulic conductivity,
- θ_r is the residual water content,
- θ_s is the saturated water content,
- b is an empirical parameter.

This equation, which illustrates how permeability changes with varying water content, indicates an increase in conductivity when the soil becomes more saturated after rainfall. These equations encompass a range of theoretical and empirical methods for characterizing clay soil permeability to changes in rainfall and moisture content. Fundamental ideas in geotechnical engineering help predict how weather changes would affect pore pressure and water flow, two factors that affect slope stability and landslide behavior. Figure 7 displays the slope model.

Figure 7 shows the maximum displacement in x direction as 0.14 m. GeoStudio generally provides better results for slope stability analysis compared to Abaqus because it is

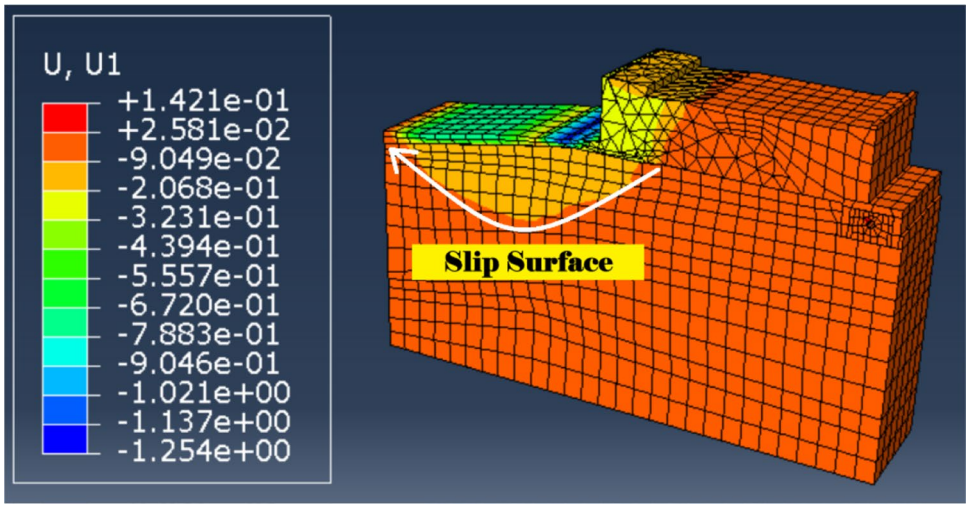

Fig. 7 Slip surface of the model (0.14 m displacement in x direction)

specifically designed for geotechnical applications, including slope stability assessments. GeoStudio incorporates specialized features for evaluating stresses, strains, and soil strength parameters that are highly relevant in such analyses. It uses limit equilibrium methods (e.g., Morgenstern-Price or Bishop's method) and FEA to provide accurate slope safety factors, while also considering complex soil behaviors like consolidation, pore pressure changes, and seepage, which are essential for realistic slope modeling. On the other hand, Abaqus is a more general-purpose FEA software, and while it can model geotechnical problems, it lacks the tailored algorithms and user-friendly tools specifically optimized for slope stability. GeoStudio's visualization tools, such as stress distribution and failure surface plots, also offer more intuitive and relevant graphical results for engineers, ensuring more accurate and reliable slope stability predictions. Therefore, the same model is analyzed using GeoStudio for further analysis. Using GeoStudio software, the same slope is modelled and analyzed in different stages, i.e., soil layers alone, soil layers with retaining wall as surcharge load, soil layers with retaining wall and light weight concrete as surcharge load and finally by adding pore water pressure to check the model stability and compute the factor of safety. Figure 8 (a, b, c, d) shows the factor of safety values in all the mentioned conditions.

Shear resistance is the soil's ability to resist forces that cause sliding along a surface or failure plane. Higher values indicate stronger resistance to shear forces, which contributes to slope stability. Shear Resistance is a function of the soil's internal properties, including cohesion and friction angle, and it directly affects the shear strength of the slope. Figure 9 shows the model coordinate system respectively. While Fig. 10 shows the graph between shear resistance vs. x-axis.

In soil permeability analysis, especially in contexts involving deep foundations like piles, the vertical permeability (k_y) and horizontal permeability (k_x) have different roles in determining the movement of groundwater and pressure changes around the foundation. The installation of piles often leads to temporary increases in pore pressure, especially in cohesive soils. Vertical permeability is essential for the dissipation of excess pore pressures induced by pile driving or loading. The presence of piles significantly impacts how important the vertical permeability is compared to the horizontal permeability. As loads are transferred through the piles into deeper soil layers, the soil around the piles

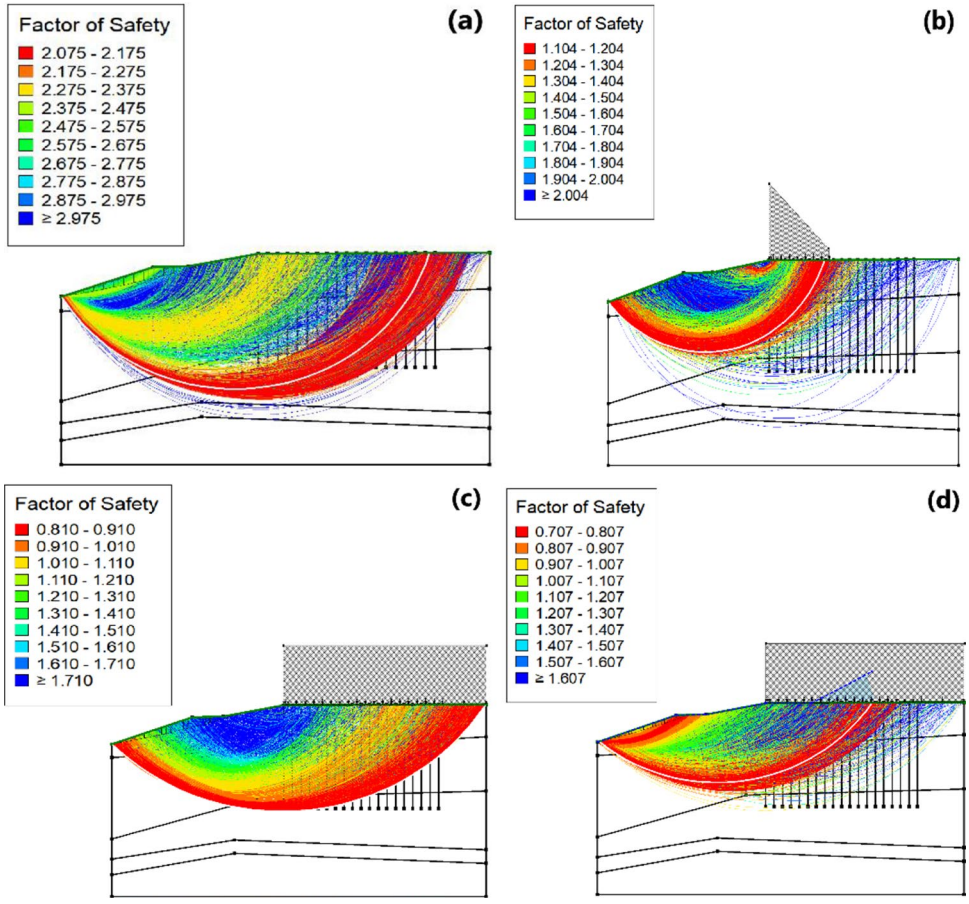

Fig. 8 (**a**, **b**, **c**, **d**) Factor of safety values in soil layers alone, soil layers with retaining wall as surcharge load, soil layers with retaining wall and light weight concrete as surcharge load and by adding pore water pressure respectively. a The slope factor of safety ranges from 2.08 to 2.18. The soil layers and slope are safe in the initial condition. b After the piles are inserted and retaining wall is built, the factor of safety ranges from 1.10 to 1.20. A small portion below the bottom corner of the retaining wall is in critical condition. c After the total load including retaining wall, light weight concrete and right-side soil is applied on the ground, the factor of safety range is then 0.81 to 0.91. A huge critical surface below the overall model is created and the slope is failed in this condition. It means the overall load exceed the strength of the soil layers 1 to 3. d Finally, after the analysis is run by adding the pore water pressure, the factor of safety ranges from 0.71 to 0.81. In reality the overall slope was failed in the same direction as mentioned in the fourth condition with pore water pressure condition

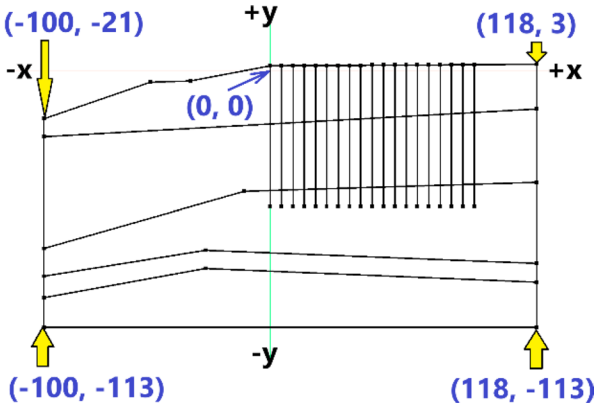

Fig. 9 Coordinate system respectively

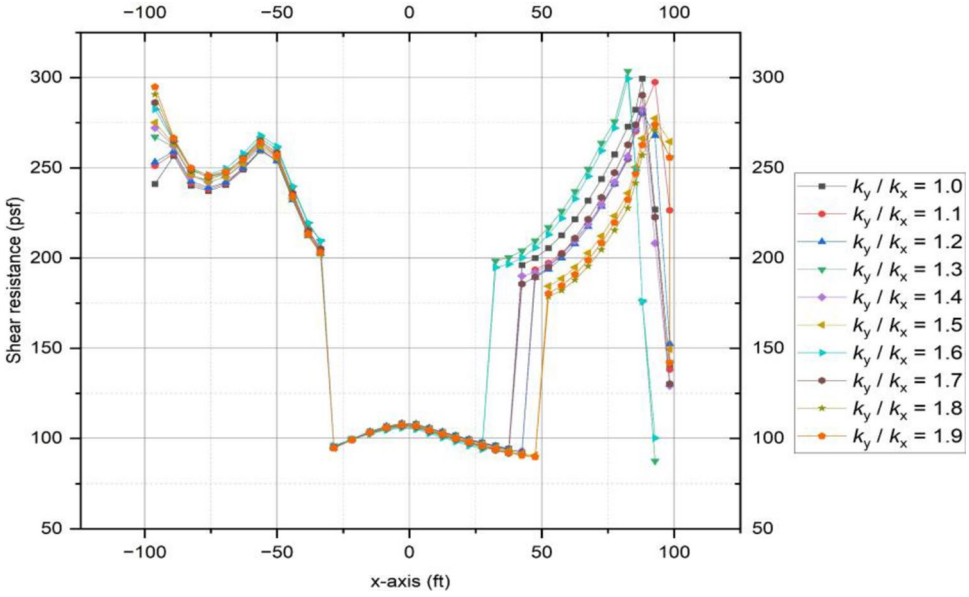

Fig. 10 Shear resistance (psf) vs. x-axis (ft) for the critical failure plane

compresses and water within the soil pores seeks an escape path. A higher vertical permeability (k_y) as compare to the horizontal permeability (k_x) is observed in this model as well. In short, while both horizontal and vertical permeability are important in the overall behavior of soil, the vertical permeability k_y gains added importance in the context of deep foundations like piles. This is due to its significant impact on drainage, consolidation, stability, and pore pressure dissipation around the pile, all of which directly influence the foundation's performance and longevity. Therefore, to check the stability analysis of the model, k_x is kept constant and k_y is changed with a ratio of k_y / k_x from 1 to 9.

Using the permeability ratio instead of the permeability magnitude in slope stability analysis is often preferred because the permeability ratio allows for a more standardized and comparative approach in terms of relative comparison, generalization across soil types, impact on slope safety and more insightful graphical analysis. The various curves represent different permeability ratios between the horizontal (k_x) and vertical (k_y) permeability. This affects how stresses propagate through the material due to permeability variation, which in turn influences its mechanical behavior under shear loading. The ratios range from 1 to 1.9, with $k_y / k_x = 1$ indicating isotropy and higher values indicating increasing anisotropy. The graph shows that the shear resistance remains relatively constant between − 100 feet and − 33 feet, maintaining values between 200 and 300 psf. Between − 33 and − 29, a sudden drop in shear resistance is observed. From − 29 to 48, the shear resistance is almost constant and maintain a value of approximately 100 psf as there are piles available as deep foundation and it took part of the resistance applied due to the load. Finally, from point 29 to 100, a sudden increase in shear resistance is observed as there is light weight concrete at the top of this area and the load is less as compare to the left side. For $k_y / k_x = 1$ (blue line), the shear resistance is generally smoother. As the permeability ratio increases (up to $k_y / k_x = 1.9$, brown line), the variations in shear resistance become more pronounced, especially near the regions of rapid shear resistance change (around 60 to 100 feet). This suggests that permeability

anisotropy influences the distribution of shear resistance, particularly in areas where there are rapid transitions in resistance, as seen at the edges of the graph. The sharp drop in shear resistance between 40 and 60 feet indicates a zone of vulnerability where the material has a reduced capacity to resist shear forces. This could correspond to areas where failure or deformation is more likely to occur. The rapid increase in shear resistance after 60 feet suggests that the material's resistance to shear improves towards the boundaries, which may reflect better material properties or less susceptibility to shear stress. This pattern of stress transition is important for understanding how the material may behave under loading conditions, and it can inform the design and safety considerations for structures or materials that are subject to shear forces.

Total normal stress refers to the total stress acting perpendicular (normal) to a surface or plane within a soil mass. This stress includes the combined effects of both the soil's weight and any external loads, such as structures or water pressure, acting vertically on the soil mass. The relationship between these components is described by the following equation:10

$$\sigma = \sigma\prime + u \tag{10}$$

Where:

- σ = Total normal stress.
- σ' = Effective stress.
- u = Pore water pressure.

Fig. 11 shows total normal stress (psf) versus x-axis (ft)

The graph demonstrates that the total normal stress increases along the x-axis, peaking around the midpoint (between −40 and 40 feet), and then begins to decrease again. This type of curve is typical in many load distribution scenarios, where the center experiences the highest total stress due to the concentration of applied loads. The stress values reach their maximum between −20 and 20 feet, and then they gradually decline, which could represent the load tapering off towards the boundaries of the system (e.g., soil section, structural element). The gradual decline in total stress on either side of the

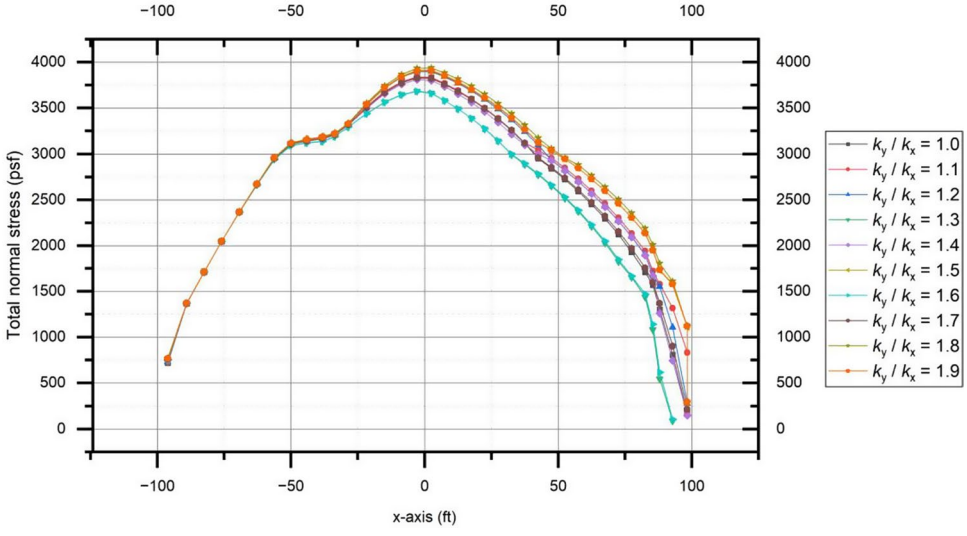

Fig. 11 Total normal stress (psf) vs. x-axis (ft) for the critical failure plane

peak suggests the outer areas are experiencing less load, or less stress is being transmitted due to the boundary effects. The rate of decline in stress towards the right side of the graph (from 60 feet onward) becomes steeper for certain k_y/k_x ratios, particularly for higher values (1.8, 1.9), suggesting that higher anisotropy could cause quicker dissipation of stress towards the edges of the system. Understanding this distribution helps in assessing how permeability anisotropy affects structural or geotechnical stability under load. From point 0 to 100, the graph shows more variations because of the presence of piles which absorbs much of the normal stress coming from the superimposed load of soil and light weight concrete.

Effective shear stress (often denoted as τ') is defined as the stress acting parallel to the failure plane, which can be calculated as the difference between total shear stress and pore water pressure. In slope stability and landsliding, it's crucial because it determines the strength of the soil or rock against sliding. Higher effective shear stress indicates greater stability. Understanding this helps engineers assess potential landslide risks and design appropriate mitigation strategies. Figure 12 shows the graph between effective shear stress (psf) vs. x-axis (ft) for permeability ratio (k_y/k_x) variation from 1 to 1.9.

The curves shown in Fig. 12 are labeled according to the ratio of permeability in the x-direction $k_x$to permeability in the y-direction k_y. This ratio affects how fluid or pressure moves through the material. Different permeability ratios are plotted to show how variations in the material's permeability in different directions (anisotropy) affect the stress distribution along the x-axis. k_y/k_x ranges from 1 to 1.9, which covers a range of isotropic (equal permeability in both directions) and anisotropic conditions (different permeabilities). At certain points of the graph (around − 40 feet and 60 feet), the effective normal stress decreases significantly, creating troughs in the graph, indicating zones of lower stress, potentially indicative of areas where less compaction or load transfer is happening. As the ratio k_y/k_x increases from 1 to 1.9, the curves show slight variations, especially around the peak stress points and the troughs. Higher permeability ratios generally lead to more pronounced shifts in stress in certain regions, particularly in the sections where the x-axis is near 80 to 100 feet and − 60 to -40 feet. Peaks (at around − 70 feet, 0 feet, and 90 feet) indicate regions where effective normal stress is highest. These areas correspond to locations where the structure or material is under higher compression or load. For k_y/k_x = 1 (blue line), which implies isotropy (equal permeability in both

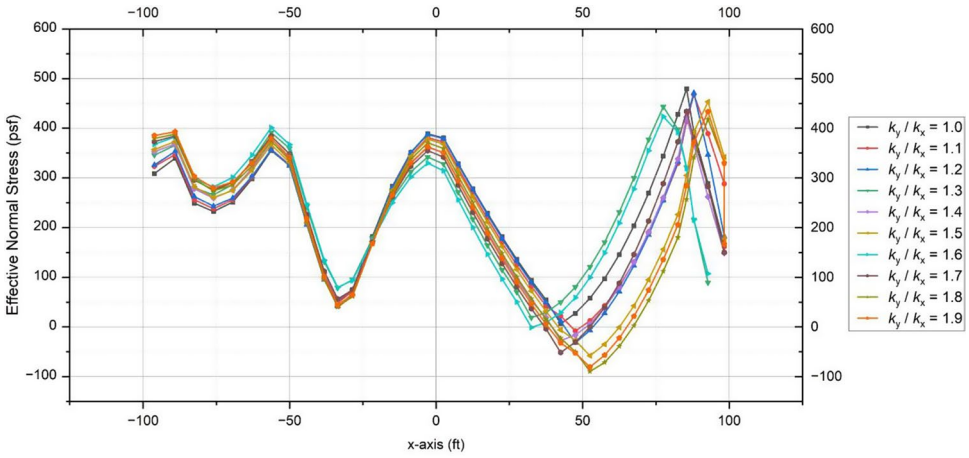

Fig. 12 Effective normal stress (psf) vs. x-axis (ft) for the critical failure plane

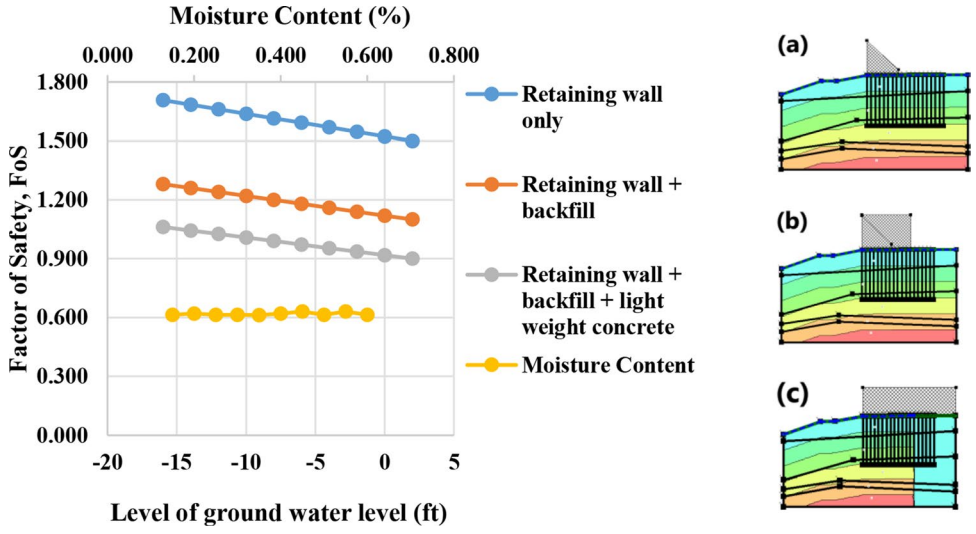

Fig. 13 Ground water level (ft) vs. FoS

directions), the stress distribution appears smoother. As k_y/k_x increases, the curves tend to deviate slightly more, indicating that anisotropy in permeability causes localized variations in stress distribution. This suggests that permeability anisotropy (when fluids or stresses pass through a material differently in different directions) has a direct impact on the stress field. The critical slope factor of safety for the permeability variations for k_y/k_x in range of 1 to 1.9 were noted in a range of 0.945 to 0.955. The overall impact of permeability and moisture content is almost negligible as the structure include too many highly congested piles (deep foundation) as supporting components. Normally the impact of permeability is higher in purely soil made slopes having no piles inserted as deep foundation. Impact of ground water level variation and moisture content on the stability of slope is shown in Figure 13.

The graph has three different lines, each representing a distinct load condition on the soil, measured in pounds per square foot (psf). Blue line (load of retaining wall only), this represents the FoS when only the surcharge load of the retaining wall itself is considered without any additional load. The blue line starts around an FoS of 1.8 at -20 feet and slightly decreases as the groundwater level rises, indicating that higher groundwater levels slightly reduce stability under this condition. But overall, the slope and model is stable in this condition. The orange line (load of retaining wall + right side soil), this represents the FoS when the soil is subjected to the load of the retaining wall plus the soil on the right side. The FoS is generally lower than the blue line, indicating that the additional soil load reduces the stability. As groundwater levels rise from − 20 to 5 feet, the FoS gradually decreases from around 1.4 to about 1.2, indicating further reduction in stability with higher groundwater levels. But in this case the slope is still safe and stable. Gray line (load of retaining wall + right side soil + lightweight concrete), this represents the FoS when the retaining wall is loaded with both the right-side soil and lightweight concrete. The gray line has the lowest FoS values, starting close to 1.0 and dropping up to 0.9 (unstable) as the groundwater level rises, indicating that this combined loading scenario has the lowest stability. Across all scenarios, as the groundwater level approaches and surpasses the reference level (moving from − 20 ft toward 5 ft), the FoS decreases. This suggests that higher groundwater levels reduce the stability of the retaining wall, likely

due to increased pore water pressure and hydrostatic forces. The stability is highest for the retaining wall alone, moderately lower when soil load is included, and lowest when both soil and lightweight concrete are added. This indicates that additional loads from adjacent soil and concrete significantly impact stability. The effect of moisture content on the FoS value is almost negligible.

Conclusion

This study investigates the critical role of soil permeability variation and groundwater dynamics in the stability of slopes reinforced by retaining walls, with a particular focus on the Huizhou slope failure. Through advanced numerical simulations and empirical field data, we have demonstrated that increasing groundwater levels, coupled with changes in soil permeability, significantly reduces the Factor of Safety (FoS) of retaining walls. Specifically, the failure observed in the Huizhou region was primarily driven by a rise in pore water pressure and reduced shear strength in the slope materials, leading to a FoS of 0.90—below the threshold for safe slope stability.

Key findings include the identification of weak silty clay layers with low shear strength parameters ($c \approx 12$ kPa, $\phi \approx 18°$), which were incapable of supporting the imposed loads. Additionally, the study reveals that permeability anisotropy and surcharge loading contribute to the amplification of stress concentrations in the slope, particularly between 40 and 60 feet, where shear forces are most critical. The influence of groundwater and permeability changes on the stability of retaining walls was clearly shown, with higher permeability accelerating pore pressure buildup, while lower permeability hindered drainage and increased hydrostatic pressure behind the retaining wall.

The findings underscore the urgent need for optimized drainage systems and accurate permeability evaluation in geotechnical design to mitigate the risks of infiltration-induced slope failure. To ensure the safety and long-term stability of slopes in high groundwater areas, engineers must consider both permeability variations and the impact of surcharge loading in their designs. This study highlights the significance of incorporating detailed soil and groundwater behavior into slope stabilization strategies and serves as a call for further research into the interaction between soil permeability, groundwater levels, and structural reinforcements.

The graphs collectively demonstrate the influence of permeability anisotropy (k_y / k_x) on stress distribution and resistance in geotechnical or structural systems. The effective normal stress and total normal stress exhibit distinct peaks and valleys, indicating regions of high and low stress concentration, with increasing anisotropy amplifying localized variations. The shear resistance graphs reveal critical zones where shear forces are concentrated or dissipated, particularly between 40 and 60 feet (x-axis), where sharp transitions occur. The findings highlight the significant impact of permeability anisotropy on both normal and shear stresses, providing crucial insights for the design and stability assessment of materials under load. The results from the graphs indicate that the permeability ratio k_y / k_x plays a crucial role in modulating both normal and shear stress distributions across the material. The effective and total normal stress profiles demonstrate that increasing anisotropy (higher k_y / k_x) causes greater stress fluctuations, particularly in regions where peaks and troughs occur, suggesting that anisotropic permeability alters the uniformity of load distribution. The shear resistance graphs emphasize zones of shear stress concentration and reduction, especially between 40 and 60

feet, which represent areas prone to structural weakness or potential failure. As k_y / k_x increases, the variations in these critical zones become more pronounced, underscoring the importance of accounting for permeability anisotropy in evaluating material stability and shear strength. These findings provide valuable insights for geotechnical and structural applications, where understanding stress behavior under varying permeability conditions is essential for ensuring material safety and performance. Quantitative assessments, such as determining the critical FoS threshold under varying conditions, should be integrated into future work to provide more comprehensive, actionable solutions for slope stability engineering.

Nomenclature

FoS	Factor of safety
E	Young's Modulus
q	Rainfall Intensity
v	Poisson Ratio
k	Permeability Coefficient
ρ_d	Dry Density
c_s	Cohesion Yield Stress
PRFs	Pile Raft Foundations
σ_t	Tension Cut-off Stress
BH	Borehole
ϕ	Friction Angle
LSS	Left Side Soil
γ	Unit Weight
F	Filter
L	Layer
k_x	Permeability in horizontal direction
UTC	Utility Tunnel Cover
k_y	Permeability in vertical direction
GB	GuoBiao (National Standard)
DBJ/T	Dìfāng Biāozhǔn Jiànzhù / Jiànzhù (Local Building Standard Code / Recommended)
FEM	Finite Element Analysis
RW	Retaining Wall
RSS	Right Side Soil

Supplementary Information

The online version contains supplementary material available at https://doi.org/10.1186/s40703-025-00238-4.

Supplementary Material 1

Supplementary Material 2

Acknowledgements
The research is funded by the National Natural Science Foundation of China (Grants No. 52178339, 52090081 and 52008261) and Shenzhen Natural Science Fund (the Stable Support Plan Program 20220808150117002).

Author contributions
Muhammad Israr Khan: Write-up, AnalysisFei Jianbo: SupervisionChen Xiangsheng: FundingChen Yue: Site data provider.

Funding
The research is funded by the National Natural Science Foundation of China (Grants No. 52178339, 52090081 and 52008261) and Shenzhen Natural Science Fund (the Stable Support Plan Program 20220808150117002).

Data availability
No datasets were generated or analysed during the current study.

Declarations

Competing interests
The authors declare no competing interests.

Received: 10 November 2024 / Accepted: 4 February 2025
Published online: 18 February 2025

References

1. Cho D-S, Kim J (2024) Stability of the front wall and the horizontal behavior of composite reinforced-earth retaining walls. Acta Geotech 19(12):8165–8176
2. Xu Y, Su C, Huang Z, Yang C, Yang Y (2022) Research on the protection of expansive soil slopes under heavy rainfall by anchor-reinforced vegetation systems. Geotext Geomembr 50(6):1147–1158
3. Wu J, Zhou Z (2023) Risk assessment of seepage failure in deep excavations based on fuzzy analytic hierarchy process and cloud model. Acta Geotech 18(10):5635–5658
4. Zhao H-j, Liu W, Shi P-x, Du J-t (2021) Chen X-m. Spatiotemporal deep learning approach on estimation of diaphragm wall deformation induced by excavation. Acta Geotech 16(11):3631–3645
5. Zhang J, Luo Y, Zhou Z, Victor C, Duan M (2021) Research on the rainfall-induced regional slope failures along the Yangtze River of Anhui, China. Landslides 18:1801–1821
6. Jayakody SHS, Uzuoka R, Ueda K, Xu J (2023) Unsaturated slopes behavior under antecedent intermittent rainfall patterns: centrifuge and numerical study. Acta Geotech 18(11):5773–5790
7. Wang S, Idinger G, Wu W (2021) Centrifuge modelling of rainfall-induced slope failure in variably saturated soil. Acta Geotech 16(9):2899–2916
8. Chen X, Zhang L, Zhang L, Zhou Y, Ye G, Guo N (2021) Modelling rainfall-induced landslides from initiation of instability to post-failure. Comput Geotech 129:103877
9. Cai F, Ugai K (2004) Numerical analysis of rainfall effects on slope stability. Int J Geomech 4(2):69–78
10. Bhattacherjee D, Viswanadham B (2018) Design and performance of an in-flight rainfall simulator in a geotechnical centrifuge. Geotech Test J 41(1):72–91
11. Tamate S, Suemasa N, Katada T (2012) Simulation of precipitation on centrifuge models of slopes. Int J Phys Modelling Geotechnics 12(3):89–101
12. Askarinejad A, Akca D, Springman SM (2018) Precursors of instability in a natural slope due to rainfall: a full-scale experiment. Landslides 15:1745–1759
13. Ng CWW, Zhan LT, Bao CG, Fredlund DG, Gong BW (2003) Performance of an unsaturated expansive soil slope subjected to artificial rainfall infiltration. Geotechnique 53(2):143–157
14. Rahardjo H, Lee T, Leong EC, Rezaur R (2005) Response of a residual soil slope to rainfall. Can Geotech J 42(2):340–351
15. Sasahara K, Sakai N (2014) Development of shear deformation due to the increase of pore pressure in a sandy model slope during rainfall. Eng Geol 170:43–51
16. Wang G, Sassa K (2001) Factors affecting rainfall-induced flowslides in laboratory flume tests. Geotechnique 51(7):587–599
17. Borja RI, White JA (2010) Continuum deformation and stability analyses of a steep hillside slope under rainfall infiltration. Acta Geotech 5:1–14
18. Damiano E (2019) Effects of layering on triggering mechanisms of rainfall-induced landslides in unsaturated pyroclastic granular soils. Can Geotech J 56(9):1278–1290
19. Fan L, Lehmann P, Zheng C, Or D (2020) Rainfall intensity temporal patterns affect shallow landslide triggering and hazard evolution. Geophys Res Lett 47(1):e2019GL085994
20. MIAO, H-b (2021) CHAI S-f, WANG G-h. influence factors for failure of cohesionless soil slopes triggered by heavy rainfall. Chin J Geotech Eng 43(2):300–308
21. WANG L, NAN F-y, WANGi S-m, LI CHENY, X-w FAN, Z-h et al (2023) Infiltration characteristics and deformation mechanism of rainfall-induced landslides in Three Gorges Reservoir Area based on 1D and 2D model tests. Rock Soil Mech 44(5):8
22. Hsu S-C, Maldonado J, Loehr E, Bowders J, Lindsey E, Omatsone W Model testing of precipitation-induced landslides. GeoCongress 2013: Stability and Performance of Slopes and Embankments III2013. pp. 426– 33
23. Locat A, Leroueil S, Bernander S, Demers D, Jostad HP, Ouehb L (2011) Progressive failures in eastern Canadian and scandinavian sensitive clays. Can Geotech J 48(11):1696–1712
24. Shan Z, Zhang W, Wang D, Wang L (2021) Numerical investigations of retrogressive failure in sensitive clays: revisiting 1994 Sainte-Monique slide, Quebec. Landslides 18:1327–1336
25. Wu L, Zhang LM, Zhou Y, Xu Q, Yu B, Liu G et al (2018) Theoretical analysis and model test for rainfall-induced shallow landslides in the red-bed area of Sichuan. Bull Eng Geol Environ 77:1343–1353
26. Hudyma N, Avar BB, Karakouzian M (2004) Compressive strength and failure modes of lithophysae-rich Topopah Spring Tuff specimens and analog models containing cavities. Eng Geol 73(1–2):179–190
27. Van Asch TW, Van Beek L, Bogaard T (2007) Problems in predicting the mobility of slow-moving landslides. Eng Geol 91(1):46–55
28. Pagano L, Picarelli L, Rianna G, Urciuoli G (2010) A simple numerical procedure for timely prediction of precipitation-induced landslides in unsaturated pyroclastic soils. Landslides 7:273–289
29. Conte E, Troncone A (2011) Analytical method for predicting the mobility of slow-moving landslides owing to groundwater fluctuations. J Geotech GeoEnviron Eng 137(8):777–784
30. Conte E, Troncone A (2012) Stability analysis of infinite clayey slopes subjected to pore pressure changes. Géotechnique 62(1):87–91
31. Bordoni M, Meisina C, Valentino R, Lu N, Bittelli M, Chersich S (2015) Hydrological factors affecting rainfall-induced shallow landslides: from the field monitoring to a simplified slope stability analysis. Eng Geol 193:19–37
32. Wu Y-m, Lan H-x, Gao X, Li L-p (2015) Yang Z-h. A simplified physically based coupled rainfall threshold model for triggering landslides. Eng Geol 195:63–69
33. Cho SE (2017) Prediction of shallow landslide by surficial stability analysis considering rainfall infiltration. Eng Geol 231:126–138
34. Lizárraga JJ, Frattini P, Crosta GB, Buscarnera G (2017) Regional-scale modelling of shallow landslides with different initiation mechanisms: sliding versus liquefaction. Eng Geol 228:346–356
35. Elia G, Cotecchia F, Pedone G, Vaunat J, Vardon PJ, Pereira C et al (2017) Numerical modelling of slope–vegetation–atmosphere interaction: an overview. Q J Eng GeolHydrogeol 50(3):249–270
36. Conte E, Troncone A (2018) A performance-based method for the design of drainage trenches used to stabilize slopes. Eng Geol 239:158–166
37. Troncone A, Pugliese L, Lamanna G, Conte E (2021) Prediction of rainfall-induced landslide movements in the presence of stabilizing piles. Eng Geol 288:106143

38. Khan MI, Wang S (2021) Slope stability analysis to correlate shear strength with slope angle and shear stress by considering saturated and unsaturated seismic conditions. Appl Sci 11(10):4568
39. Khan MI, Wang S (2021) Slope Stability Analysis to develop correlations between different soil parameters and factor of Safety using regression analysis. Pol J Environ Stud.;30(5)
40. Wang S, Khan MI (2021) Developing correlations for Advance prediction of slope factor of Safety using Linear regression analysis–Karachi Landslide as a case study. Pol J Environ Stud 30(6):5849–5862
41. Khan MI, Wang S (2021) Method for predicting factor of safety and seepage due to variation in dam width and other parameters. Proceedings of the Institution of Civil Engineers-Geotechnical Engineering.;176(2):157–65
42. Khan MI, Wang S (2023) Initial risk Assessment to find risky slopes. J Appl Sci Eng 26(11):1597–1608
43. Khan MI (2023) Correlations between factor of safety with distributed load and crest length–Zariwam landslide as case study. Geology, Ecology, and Landscapes.:1–14
44. Khan MI, Wang S, Wang P, Nikjow MA (2022) Soil slope analysis to develop useful correlations in saturated and unsaturated conditions. Proceedings of the Institution of Civil Engineers-Forensic Engineering.;177(1):14–22
45. Khan MI, Wang S (2022) Dynamic deformation analysis of the upstream and downstream slope of the rockfill nauseri dam. J Appl Sci Eng 26(2):293–301
46. Khan MI, Wang S (2022) Develop correlations between soil parameters: Jandola Pakistan landslide as case study. Proceedings of the Institution of Civil Engineers-Forensic Engineering.;175(3):78–86
47. Khan MI, Wang S (2022) Correlating groundwater level and shear strength: Kotkai Pakistan landslide as case study. Proceedings of the Institution of Civil Engineers-Forensic Engineering.;175(1):21–7
48. Hemeda S (2024) PLAXIS 3D numerical analysis of complex geotechnical problems of colossal built heritage. Herit Sci 12(1):32
49. Pradeep T, Kumar DR, Kumar N, Wipulanusat W, Keawsawasvong S, Sunkpho J (2024) Performance evaluation and Triangle Diagram of Deep Learning Models for Embedment depth prediction in cantilever sheet piles. Eng Sci 28:1082
50. Location (2024): https://maps.app.goo.gl/7FDZqRkB6Tu3eQfy6
51. GB50021 (2001) Code for investigation of geotechnical engineering, National standard of the People's Republic of China
52. 15-60-2019 DT (2019) Code for Testing of Building Foundation

Publisher's note

Springer Nature remains neutral with regard to jurisdictional claims in published maps and institutional affiliations.